Eur. Phys. J. B **24**, 541–547 (2001)

THE EUROPEAN PHYSICAL JOURNAL B

EDP Sciences

Test of the universality of the critical adsorption profile by neutron reflection

J. Jestin[1], L.-T. Lee[2], M. Privat[3], and G. Zalczer[1,a]

[1] Service de Physique de l'État Condensé, C.E.N. Saclay, 91191 Gif-sur-Yvette, France
[2] Laboratoire Léon Brillouin, C.E.N. Saclay, 91191 Gif-sur-Yvette, France
[3] UMR 6521, U.B.O., 6 avenue Victor Le Gorgeu, 29285 Brest, France

Received 30 May 2001

Abstract. Using neutron reflectivity, we directly and self-consistently obtained all the parameters of the critical adsorption profile of three critical mixtures (n-hexane+perfluorohexane, deuterated methanol+cyclohexane and methanol+deuterated cyclohexane) assuming only a Liu-Fisher form for the profile. The characteristic exponent and the amplitude ratio which can be deduced from the neutron spectra alone are in good agreement with one another, with ellipsometric data and with theoretical values. Owing to auxiliary measurements of coexistence curves and correlation lengths, we could also check the amplitude of the intermediate and distal parts of the profile with good agreements for the methanol cyclohexane mixtures only. The adsorbed amount is much greater in the n-hexane+perfluorohexane mixture where both the power-law amplitude and the characteristic length of the profile are affected.

PACS. 68.03.-g Gas-liquid and vacuum-liquid interfaces – 64.60.Fr Equilibrium properties near critical points, critical exponents

Introduction

The problem of critical adsorption has received constant attention over many years from both experimental and theoretical points of view. However the difficulties are such that it is still considered as a challenge with many unanswered questions. It has long been recognized that the equilibrium state of a mixture (of molecules A and B, of molecules A and voids, of up and down spins) is modified close to the edge of a sample [1] (solid wall or vapor). It has also been recognized that when the mixture exhibits a critical point, critical laws can describe its properties in a wide area of the phase diagram with a more dramatic effect close to the critical point [2]. Moreover the critical laws are universal: denoting m the order parameter (a density which is zero at the critical point and spontaneously becomes finite when the temperature T is changed into the low symmetry region of the phase diagram) and t the reduced temperature defined as $t = (T - T_c)/T_c$ (T_c is the critical temperature), the spontaneous symmetry breaking can be written as: $m = B|t|^\beta$, where the exponent β is universal *i.e.* it depends only on the space dimensionality (d) and the number of components (n) of the order parameter. In fluid systems, $d = 3$ and $n = 1$ with $\beta \approx 0.325$ [2].

The amplitude B is system dependent but related to the amplitudes of other critical laws so that there are only two independent amplitudes for a bulk system. The order parameter profile close to a wall also obeys a universal function. From very general scaling arguments, when the field which creates the profile is strong enough, Fisher and De Gennes [3] determined the limiting behaviors:

$$m \propto z^{-\zeta} \quad \text{with} \quad \zeta = \beta/\nu \quad \text{for} \quad z < \xi \qquad (1)$$

$$m \propto \exp(-z/\xi) \quad \text{for} \quad z \to \infty \qquad (2)$$

where z is the distance from the wall and ξ the correlation length (which behaves as $\xi = \xi_0 t^{-\nu}$ with $\nu \approx 0.63$). Liu and Fisher [4] proposed an interpolation formula, governed by the crossover parameter c:

$$m = A|t|^\beta (\xi/z + c)^{\beta/\nu} \exp(-z/\xi) \qquad (3)$$

c being also a universal number. According to scaling, the amplitude A is related to that of the coexistence curve B by a universal proportionality constant P_∞. The leading amplitude of the large z behaviour is therefore $P_\infty = P_0 c^{\beta/\nu}$. Liu and Fisher deduced from the available optical experimental data a first value of $c \approx 0.7$ corresponding to $P_0/P_\infty \approx 1.18$. Subsequently, two different theoretical determinations were performed using renormalization group techniques (RG) [5] and Monte-Carlo simulation (MC) [6] but the computed functions were published later [7]. The amplitudes corresponding to these profiles have been quoted without explicit derivation. These are $P_0 = 0.866$, $P_\infty = 1.5$, $P_0/P_\infty = 0.577$, $c = 2.8$

[a] e-mail: zalczer@spec.saclay.cea.fr

for MC and $P_0 = 0.717$, $P_\infty = 1.621$, $P_0/P_\infty = 0.442$, $c = 4.8$ for RG. We also obtained very good fits of the data of reference [7] using the Liu-Fisher function but with different values of c: $c = 2.27$ ($P_0/P_\infty = 0.65$) for MC. A simple plot of the RG data hardly departs at the smallest available z from the large z exponential limit, indicating a much larger value of c. The values found depend strongly on minute details of the fitting process: for example, a constant absolute uncertainty leads to $c = 11$ while a constant relative uncertainty leads to $c = 25$. A more refined theoretical computation [8] using interpolation between 2 dimensional Ising model and $4 - \epsilon$ expansion provides $P_0 = 0.94 \pm 0.05$.

Until very recently, most experimental investigations of the adsorption layers used optical techniques: reflectometry [9–12], ellipsometry [7,13–31] or evanescent wave induced fluorescence [32,33]. The length scale of these probes is that of the wavelength of light, which is always much larger than the critical correlation length and the adsorption profile width. Surface tension [34–41] or gravimetric measurements [42,43] suffer the same limitation. A comprehensive review of experimental data [8] shows values for P_0 ranging from 0.77 to 1.6 and a weighed mean of 0.955 ± 0.08. Another review of ellipsometric data [7] focusing on P_0/P_∞ leads to $P_0/P_\infty = 0.75 \pm 0.17$. Carpenter *et al.* [44,45] recently proposed a different crossover scheme which fits the ellipsometric data better but is not continuous in all derivatives.

Only recently have tests on a smaller scale been attempted using neutron reflectivity. Zhao *et al.* [46] obtained three spectra with the methanol+deutered cyclohexane mixture from which they extracted ambiguous values of the amplitudes. They also noticed, but did not take properly into account, the attenuation of the neutron beam at the menisci (see below). Howse *et al.* [47] applied the method suggested by Dietrich and Schack [48], which gives access only to the asymptotic part of the profile at criticality, and obtained a consistent value for the exponent and a puzzling value for the amplitude. The strong field assumption has also been put to test [49,50] and shown to hold except for very special cases where this factor could change sign and therefore cross through small values. In this case theoretical investigations have led to the introduction of a second length and a non-monotonic profile [51–53].

Experiment

We studied three mixtures: n-hexane and perfluorohexane (FH), deuterated methanol and cyclohexane (CM*) and methanol and deuterated cyclohexane (MC*). The adsorbed perfluorohexane-rich or deuterated methanol rich layers act as a repulsive barrier for neutron refraction and the reflectivity is enhanced; while the hydrogenated methanol rich layer smooths the potential step and reduces the reflectivity. Dietrich and Schack [48] showed that in the first case, close to the critical point, the reflectivity reaches 1 at the critical wavelength with zero slope (the total reflection plateau appears widened) and the profile exponent could be deduced from the shape of the curve. For the second case, Zhao *et al.* [46] established that the power law tail of the profile caused a step in the reflectivity curve at the total reflection threshold.

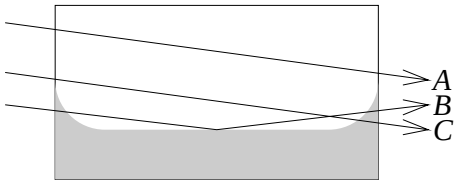

Fig. 1. Schematic side view of the experimental setup showing that at grazing incidence, the incident and reflected beams (B) must cross through a finite thickness of liquid when the meniscus is directed upwards. The reference beam (A) is obtained by lowering the whole thermostat so that it crosses through the same windows. Measurements at different cell heights in the C position allow the determination of an analytic formula for the attenuation (Eq. (6)) with which reflexion spectra can be corrected.

Perfluorohexane and n-hexane were obtained from Aldrich (99+ % and 99% purity, respectively), cyclohexane and methanol from Merck (99.8% purity), and deuterated cyclohexane and methanol from Eurisotop (99.8% purity). All the products were used as received and the samples were prepared by weighing in a nitrogen filled inflatable glove bag. The critical concentrations were obtained from our own coexistence data (see Tab. 2) or reference [54]. The fused silica cell was fitted with a leak-proof Rotaflo stopper and placed in a bulky thermostat with a temperature stability of ± 0.01 K. We did not notice any evolution of the samples during the experiment.

The neutron reflectivity spectra were recorded at the DESIR facility of the ORPHEE reactor at the Laboratoire Léon Brillouin in Saclay. The wavelength analysis is performed by a time-of-flight technique. The incidence angle is set by deviating the neutron beam using a supermirror. The range of useful neutron wavelengths extends from 0.5 nm to 2 nm. The incidence angles were chosen in order to place the total reflection critical wavelengths at around 1.5 nm. The setup is sketched in Figure 1. As can be seen from the figure, the incident and reflected neutron beams have to cross a non-negligible thickness of liquid at the wetting menisci with significant attenuation having a marked wavelength dependance [55]. We did not succeed in inverting the meniscus by coating the walls or using other materials. We could reduce the thickness crossed by increasing the length of the cell to 20 cm. Due to this effect, the measured value for reflection at the total reflection plateau (ratio of B to A in Fig. 1) was about 0.7 for FH and MC* (compared to about 0.1 for the case of Ref. [47]) and 0.1 for CM*. The spectra can be corrected with the help of auxiliary transmission measurements (beam C in Fig. 1). Optical turbidity monitoring through the narrower side (2 cm) of the sample allowed the approach of T_c to be detected.

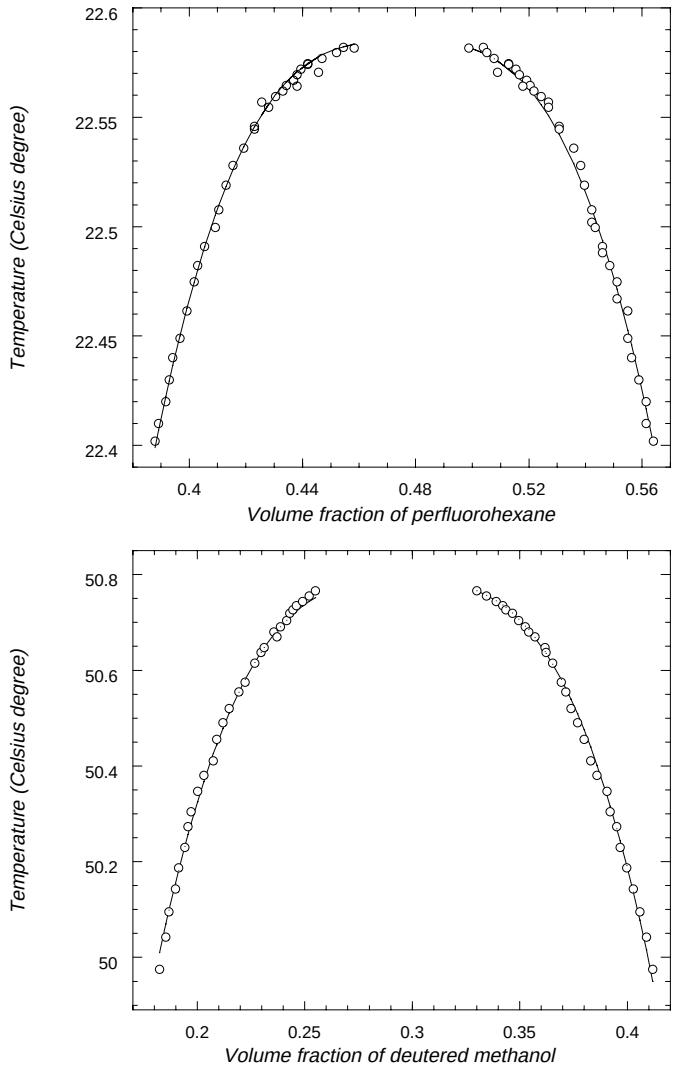

Fig. 2. Phase diagrams of FH and CM* systems near the consolute point. Open circles are the data points. Solid lines, deduced from the universal law: $m = B|t|^{\beta}$, allowed us to extract amplitude values of $B = 0.96$ for the FH mixture and $B = 0.80$ for the CM* mixture.

Auxiliary measurements

In order to compare the adsorption profile amplitudes with their bulk counterparts, we performed measurements of coexistence curves and determined the correlation length using dynamic light scattering (DLS) and viscosity measurements. The coexistence curves were determined through refractive index measurements in the two-phase region. Results are reported in Figure 2 for the FH and the CM* mixtures. A square fused silica cell was immersed in a thermostated water bath and the deviation of a laser beam passing through the corner (minimum deviation method) monitored at different temperatures. The conversion from refractive index to concentration was done using the Lorentz-Lorenz formula cross-checked using known concentration samples.

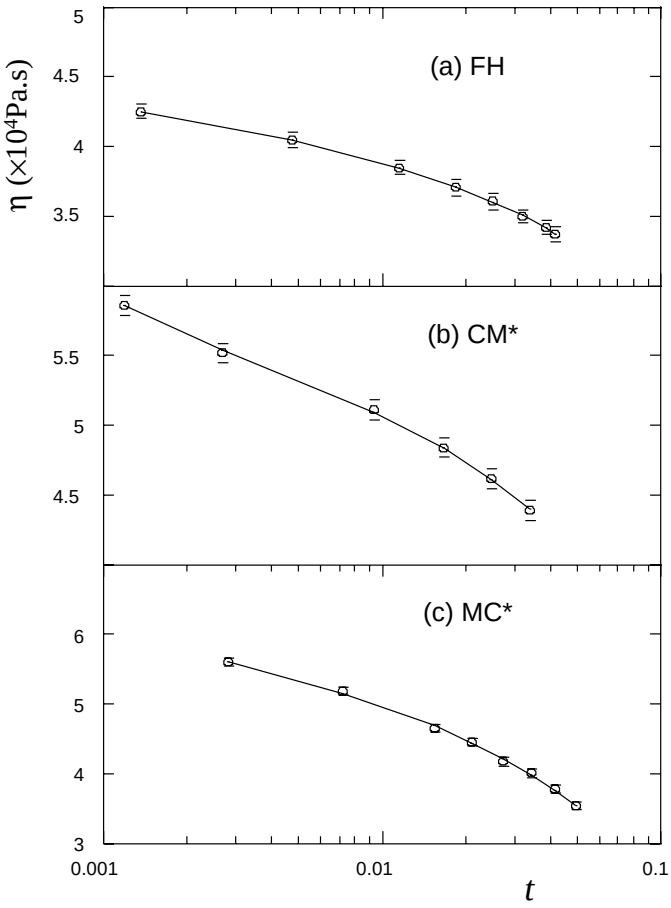

Fig. 3. Viscosity measurements *versus* the reduce temperature t. Open circles are data points and solid lines could be deduced from equation (4).

The exact relation between "static" and "dynamic" correlation lengths is still an open question, but we are mainly interested in comparing sets of data. DLS was performed with high quality cylindrical cells placed in a temperature controlled index matching fluid (decalin). Homodyne photon counting was used. The correlation function was computed using a BI2030 digital correlator with sample times down to 0.1 μs. At each temperature, correlation functions were recorded at different angles and different sample times. No departure from exponential form was observed and the characteristic times τ obeyed a q^{-2} dependence. The correlation length can be deduced from the modified Einstein-Stokes law [56]:

$$\tau = 5\pi\eta\xi/k_{\mathrm{B}}Tq^2 \qquad (4)$$

The viscosity was measured by a capillary flow technique using a leakproof cell in a water thermostated bath. Since the time of flow was very long, we recorded the image of the reservoir with a video recorder, which allowed a precise delayed measurement. The data, reported in Figure 3, were well fitted by the usual law [57]:

$$\eta = \eta_0|t|^{-y_\eta}\exp(W/T) \qquad (5)$$

where $y_\eta \approx 0.04$. The correlation length ξ, deduced from equations (4) and (5), exhibited a critical behavior which

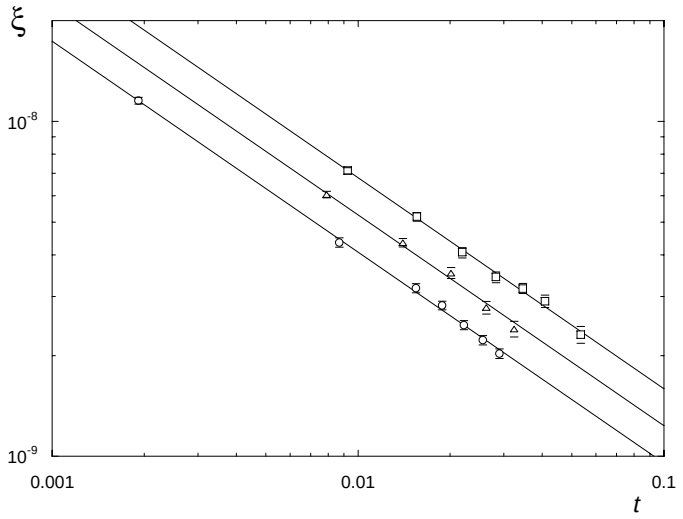

Fig. 4. Correlation lengths measured by dynamic light scattering in the FH mixture (circles), the CM* mixture (triangles) and the MC* mixture (squares). Solid lines have a slope of $\nu = 0.63$.

could be written as $\xi = \xi_0|t|^{-\nu}$ with $\nu \approx 0.63$ (Fig. 4). The attenuation of the neutron beam crossing the menisci of the mixture is due to the scattering by the fluctuations of the coherent diffusion length. Indeed we found that the attenuation by the mixtures was much larger than that observed for each of the components, even the hydrogen rich one, which excludes inelastic effects. We fitted successfully the transmission data with the law

$$\ln(I_{\rm tr}/I_0) \propto -l\lambda^2 \ln(1 + \Lambda^2/\lambda^2) \qquad (6)$$

obtained by integrating the usual Ornstein-Zernicke scattering cross-section over all solid angles where l is the thickness and Λ a characteristic length depending on the fluid. This attenuation is independent of the temperature in our range and Λ is much smaller than the critical correlation length and is of the order of a few molecular sizes. It is probably related to the short range part of the correlation function. Equation (6), with the corresponding value of Λ, was used for correcting the reflection spectra.

Data analysis

Sets of spectra were recorded at temperatures ranging from a few tens of millikelvin to about 10 kelvin above the critical temperature. The method of Dietrich and Schack [48] for determining directly the exponent ζ is not relevant for the MC* case. For the other mixtures, we observed a power law similar to that expected only rather far from the threshold, while it is expected to hold in its vicinity (although it is blurred by the finite resolution of the apparatus). It also only allows the determination of the parameters of the power-law part of the profile.

A minimal model which could describe all the data must include, in addition to the limiting power law behaviour, an exponential decay at long distance and some way of bridging these limiting laws. We preferred to use a more standard least square fitting technique and determine the best values for all the parameters. The sets of data computed either by renormalization group theory [5] or Monte-Carlo simulation [6] are also both well fitted by the formula of Liu and Fisher. This formula is obviously a most sensible way to interpolate and extrapolate the discrete values in order to yield the continuous profile required for numerical integration. The quality of the fit validates the Liu Fisher formula as a suitable way of bridging both asymptotic behaviors in the intermediate range. The profiles proposed by Carpenter *et al.* [44,45] are also similar but more complicated to compute.

Of course the divergence of the power law close to the interface was cut-off at the pure component concentration value. Model spectra were therefore computed by numerically integrating the Schrödinger equation obeyed by the neutrons in the potential imposed by the Liu-Fisher concentration profile. This integration was performed using a quality-controlled fourth order Runge-Kutta algorithm [58]. This routine was then included in a non-linear minimization program based on the Nelder-Mead simplex algorithm [58]. The fitting procedure is very long and delicate, considering the large number of adjustable parameters. Some of these parameters are characteristic of the system and should be the same for all spectra. This occurs for the parameters of the profile (exponent ζ, crossover c, amplitude A) or of the bulk system (critical temperature $T_{\rm c}$, correlation length amplitude ξ_0) or of the experimental setup (incidence angle, wavelength resolution, noise level). The thickness of liquid crossed at the menisci and the overall norm, which varied slightly when changing the temperature, could be fitted by a nested linear minimization routine. Fitting each spectrum separately was pointless, equal quality fits can be obtained with quite different sets of parameters, the variation of one of them being compensated by the variations of the others. Also some spectra contain more information on a given parameter and little on another. For instance, the spectra close to $T_{\rm c}$ are more sensitive to the profile but the determination of these parameters requires knowledge of the total reflection threshold which cannot be determined from the same spectrum (in the repulsive case). We therefore simultaneously fit all the spectra of a given set together.

Due to this complexity, the fitting program was repeatedly trapped in local minima. To overcome this problem, we systematically varied each parameter in turn around its previous best value, and fitted all the other parameters while monitoring the resulting χ^2, until we obtained a stable minimum. The three parameters related to the setup quickly reached stable values and were then fixed.

Results and discussion

The best fits of the neutron experiments are reported in Figures 5–7. For clarity only one deviation curve has been plotted for each sample but no systematic distortion was visible at any temperature.

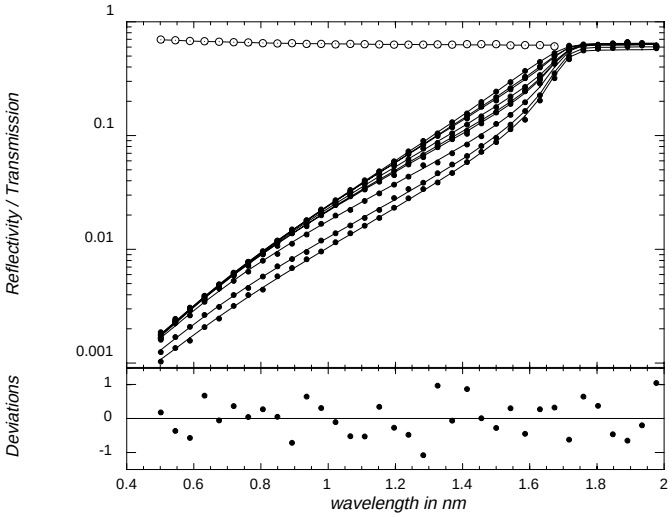

Fig. 5. The nine spectra recorded (full dots) for the FH mixture with the computed curves (lines). The temperatures are, from bottom to top, 30 °C, 27 °C, 24.35 °C, 23.35 °C, 23.20 °C, 23 °C, 22.85 °C, 22.80 °C and 22.71 °C. The top curve (open circles) is the interpolated attenuation in the menisci. In the lower frame a typical relative deviation of a computed spectrum from its experimental counterpart is drawn.

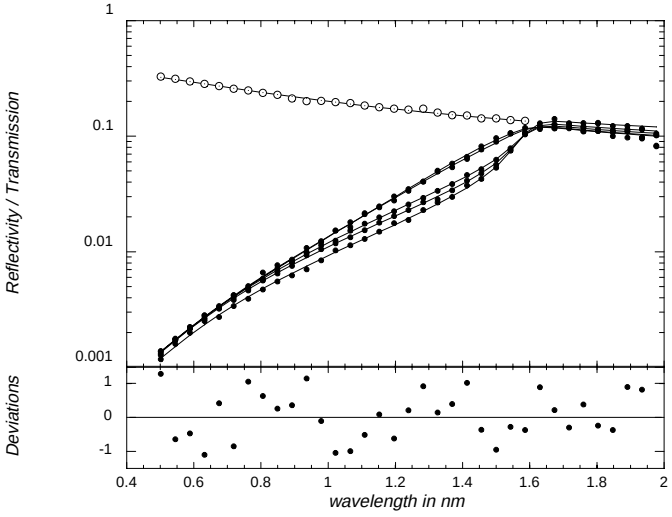

Fig. 6. The five spectra recorded (full dots) for the CM* mixture with the computed curves (lines). The temperatures are, from bottom to top 55 °C, 54 °C, 53.5 °C, 52.8 °C and 52.73 °C.

In order to estimate uncertainties, we plotted the values of χ^2 obtained when scanning the parameters. The case of ζ is depicted in Figure 8. The quoted uncertainties are then defined by an increase of 1 of the χ^2 graphically determined by the lower envelope of all best χ^2. This procedure leads, however, to narrower intervals compared with the usual definition of errors bars.

The final results are reported in Table 1. Results deduced from auxiliary measurements are reported in Table 2. Some of the numbers are redundant: they express

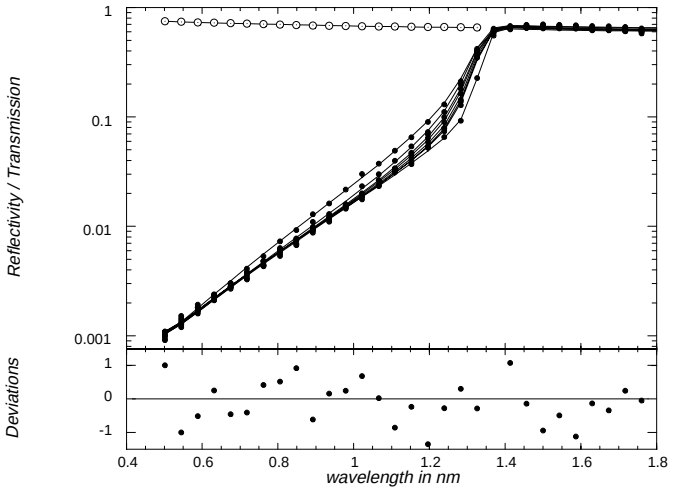

Fig. 7. The eight spectra recorded (full dots) for the MC* mixture with the computed curves (lines). The temperatures are, from top to bottom 50 °C, 45.5 °C, 45 °C, 44.7 °C, 44.5 °C, 44.4 °C, 44.3 °C and 44 °C.

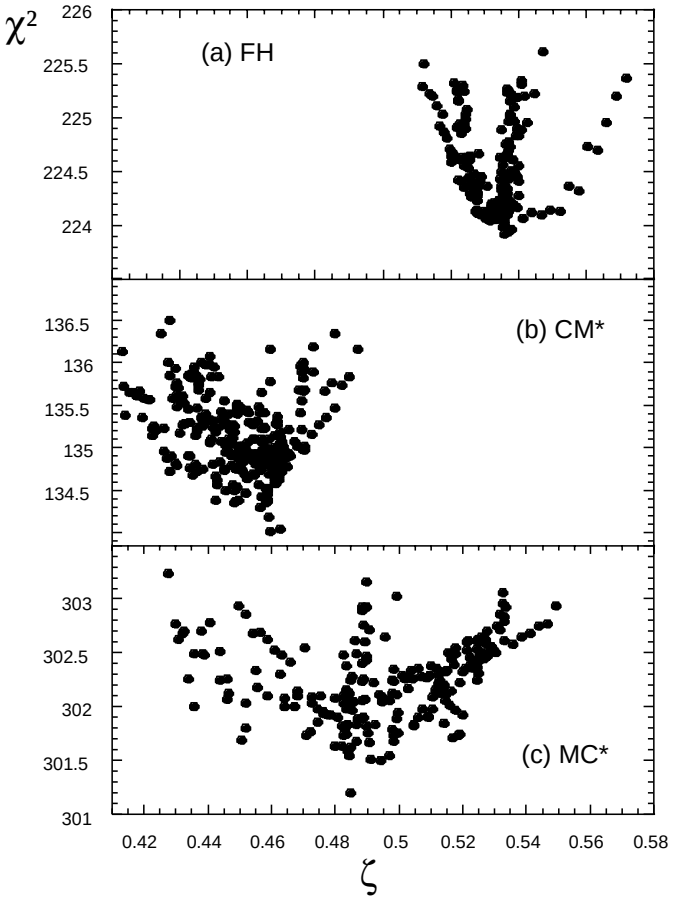

Fig. 8. χ^2 (sum of the squared relative deviations for 315 data points for the FH mixture, 175 data points for the MC* mixture and 280 data points for the CM* mixture) for different fits *versus* the exponent. All the point lie above a parabolic curve with a minimum at $\beta/\nu = \zeta \approx 0.54$ and increase by 1 when ζ is changed by ± 0.025 for the FH, a minimum at $\zeta \approx 0.46 \pm 0.03$ for the MC* and a minimum at $\zeta \approx 0.48 \pm 0.05$ for the CM* mixture.

Table 1. Critical adsorption parameters.

	FH	CM*	MC*
ζ	0.54 ± 0.03	0.46 ± 0.03	0.49 ± 0.05
c	1.68 ± 0.4	4.8 ± 2.0	3.2 ± 1.6
A	1.71 ± 0.20	0.75 ± 0.14	0.70 ± 0.14
ξ_0 (nm)	0.27 ± 0.01	0.29 ± 0.02	0.36 ± 0.01
P_0/P_∞	0.76 ± 0.1	$0.49^{+0.15}_{-0.07}$	$0.57^{+0.03}_{-0.07}$
P_∞	2.34±0.2	$1.91^{+0.2}_{-0.35}$	$1.71^{+0.4}_{-0.3}$
P_0	1.78 ± 0.2	0.94 ± 0.15	0.97 ± 0.15
a (nm)	2.37	0.336	0.336

Table 2. Auxiliary measurements parameters. For the MC* mixture, B_ϕ and ϕ_c values are taken from [54].

	FH	CM*	MC*
ϕ_c	$0.47^F \pm 0.005$	$0.70^C \pm 0.005$	$0.718^{C*} \pm 0.005$
B_ϕ	0.96 ± 0.01	0.80 ± 0.01	0.713 ± 0.01
ξ_0 (nm)	0.22 ± 0.01	0.29 ± 0.03	0.37 ± 0.02
$\eta_0(\mu$Pa.s)	19.50 ± 1	8.06 ± 0.5	0.33 ± 0.02
W (K)	839 ± 20	1298 ± 50	2279 ± 50
Λ (nm)	0.48 ± 0.05	1.8 ± 0.05	1.1 ± 0.05

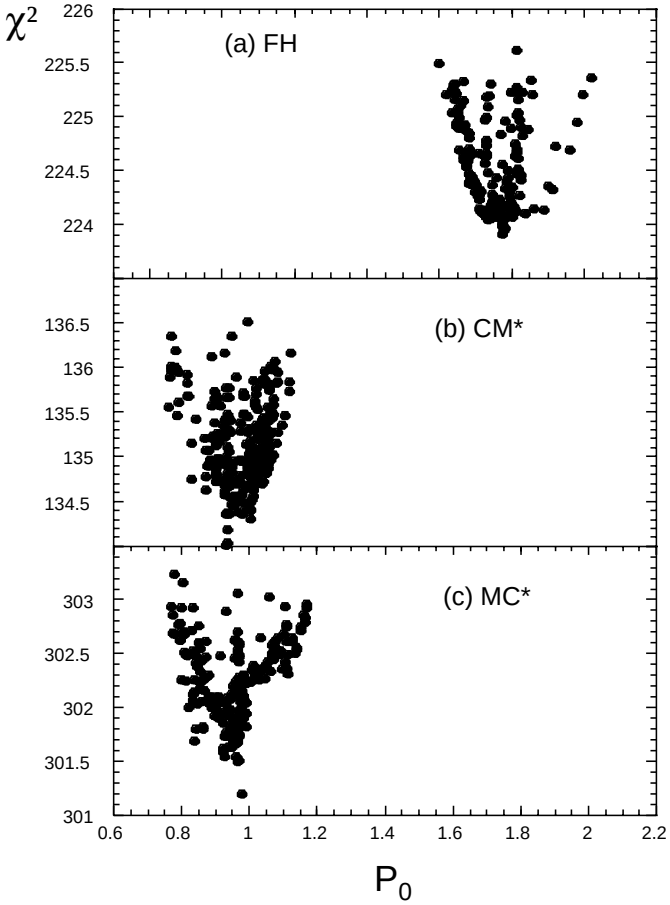

Fig. 9. Same as Figure 8 with P_0 as abscissa. The acceptable range of P_0 for FH do not overlap that of the other mixtures.

the same results in different ways. For instance, the ratio P_0/P_∞ is simply related to ζ and c through $P_0/P_\infty = c^{-\zeta}$. These relations are not linear so that computing averages depends on which aspect is considered. According to the scaling theory, the exponent and the amplitudes P_0, P_∞ and therefore their ratio P_0/P_∞ should be the same for all mixtures. The χ^2 plots for ζ and P_∞ support this prediction. The value of the exponent ζ is in very good agreement with the expected value of $\beta/\nu \approx 0.52$. However, a serious discrepancy is evident (Fig. 9) in the case of P_0. Both cyclohexane-methanol mixtures exhibit values in very good agreement with the theoretical expectation while the value for FH is almost twice as big. The value of ξ_0 in the profile of the FH mixture is also different from that obtained by DLS while the agreement is excellent in the other mixtures. It should be noted that these discrepancies contribute cumulatively when considering the distance a at which the profile reaches the pure component: 2.37 nm for FH, compared with 0.336 nm for the other mixtures. The overall adsorption is much greater in this case and this is probably related to the fact that the difference of the surface tensions of the two components of the mixture is bigger. In the review of Flöter and Dietrich [8] two experiments [12,21] already reported values of P_0 distinctly higher than the average. One may therefore ask whether the universality of the saturated regime should not be questioned.

Conclusion

Neutron reflectivity proves to be a very powerful tool for studying adsorption processes. Within the framework of Liu-Fisher theory, it provides for an independent determination of all the relevant parameters. The exponent ζ is found to be in good agreement for different mixtures and with theoretical predictions. The amplitudes P_0 and P_∞ measured in both methanol cyclohexane mixtures also show the same agreement (even though their ξ_0 are very different). However, the adsorption is much more important in the perfluorohexane-hexane mixture than that inferred from the universality hypothesis; the power-law amplitudes, P_0 and P_∞, the characteristic lengths, a and ξ_0, are also bigger. Therefore, there might be exceptions to the universal character of the strong field adsorption profile. This demonstration of the potential of this technique also opens the way to significant studies of non-critical adsorption or prewetting.

We gratefully acknowledge fruitful discussions with Alain Menelle and Gerard Janninck. This work was supported in part by Agence de l'Environnement et la Maîtrise de l'Énergie.

References

1. The collected works of J.W. Gibbs (Longmans Green, New York, 1931).
2. See *e.g.* H.E. Stanley, *Introduction to phase transitions and critical phenomena* (Clarendon Press, Oxford, 1971) or M.A. Anisimov, *Critical phenomena in liquids and liquid crystals* (Gordon and Breach, 1991).
3. M.E. Fisher, P.-G. De Gennes, C. R. Acad. Sci. Paris B **287**, 207 (1978).
4. A.J. Liu, M.E. Fisher, Phys. Rev. A **40**, 7202 (1989).
5. H.W. Diehl, M. Smock, Phys. Rev. B **47**, 5841 (1993).
6. D.P. Landau, K. Binder, Phys. Rev. B **41**, 4786 (1990); M. Smock, H.W. Diehl, D.P. Landau, Ber. Bunsenges. Phys. Chem. **98**, 486 (1994).
7. D.S.P. Smith, B.M. Law, M. Smock, D.P. Landau, Phys. Rev. E **55**, 620 (1997).
8. G. Flöter, S. Dietrich, Z. Physik B **97**, 213 (1995).
9. C. Franck, S.E. Schnatterly, Phys. Rev. Lett. **48**, 763 (1982).
10. J.A. Dixon, M. Schlossman, X.-L. Wu, C. Franck, Phys. Rev. B **31**, 1509 (1985).
11. C. Franck, J. Chem. Phys. **82**, 5633 (1985).
12. M. Schlossman, X.-L. Wu, C. Franck, Phys. Rev. B **31**, 1478 (1985).
13. D. Beaglehole, J. Chem. Phys. **73**, 3366 (1980).
14. D. Beaglehole, J. Chem. Phys. **75**, 1544 (1981).
15. D. Beaglehole, Phys. Lett. A **91**, 237 (1982).
16. D. Beaglehole, J. Phys. Chem. **87**, 4749 (1983).
17. B. Heidel, G.H. Findenegg, J. Phys. Chem. **88**, 6575 (1984).
18. B. Heidel, G.H. Findenegg, J. Chem. Phys. **87**, 706 (1987).
19. R. Süssmann, G.H. Findenegg, Physica A (Amsterdam) **156**, 114 (1989).
20. A. Hirtz, W. Lawnik, G.H. Findenegg, Colloids Surf. **51**, 405 (1990).
21. A. Hirtz, K. Bonkhoff, G.H. Findenegg, Adv. Colloid Interface Sci. **44**, 241 (1993).
22. J.W. Schmidt, M.R. Moldover, J. Chem. Phys. **83**, 1829 (1985).
23. J.W. Schmidt, J. Chem. Phys. **85**, 3631 (1986).
24. J.W. Schmidt, Phys. Rev. A **41**, 885 (1990).
25. D. Bonn, H. Kellay, G.H. Wegdam, J. Chem. Phys. **99**, 7115 (1993).
26. B.M. Law, Phys. Rev. Lett. **67**, 1555 (1991).
27. B.M. Law, C.M. Sorensen, F. Zhou, Fluid Phase Equilibria **75**, 225 (1992).
28. D.S.P. Smith, B.M. Law, J. Chem. Phys. **99**, 9836 (1993).
29. D.S.P. Smith, B.M. Law, Phys. Rev. E **52**, 580 (1995).
30. D.S.P. Smith, B.M. Law, Phys. Rev. E **54**, 2727 (1996).
31. C.L. Caylor, B.M. Law, J. Chem. Phys. **104**, 2070 (1996).
32. D. Beysens, L. Leibler, J. Phys. France Lett. **43**, L133 (1982).
33. G. Zalczer, J. Phys. France **47**, 379 (1986).
34. M.P. Khosla, B. Widom, J. Colloid Interface Sci. **76**, 375 (1980).
35. N. Nagarajan, W.W. Webb, B. Widom, J. Chem. Phys. **77**, 5771 (1982).
36. M. Privat, L. Tenebre, R. Bennes, E. Tronel-Peyroz, J.M. Douillard, L. Gaicha, Langmuir **4**, 1151 (1988).
37. L. Gaicha, M. Privat, L. Tenebre, R. Bennes, E. Tronel-Peyroz, J.M. Douillard, Langmuir **4**, 1326 (1988).
38. R. Bennes, M. Privat, E. Tronel-Peyroz, M. Amara, Langmuir **7**, 1088 (1991).
39. M. Amara, M. Privat, R. Bennes, E. Tronel-Peyroz, Europhys. Lett. **16**, 153 (1991).
40. M. Amara, M. Privat, R. Bennes, E. Tronel-Peyroz, J. Chem. Phys. **98**, 5028 (1993).
41. S. Karad, M. Amara, A. Louenan, E. Tronel-Peyroz, R. Bennes, M. Privat, J. Chem. Phys. **100**, 1498 (1994).
42. S. Blümel, G.H. Findenegg, Phys. Rev. Lett. **54**, 447 (1985).
43. G.H. Findenegg, R. Löring, J. Chem. Phys. **81**, 3270 (1984).
44. J.H. Carpenter, B.M. Law, D.S.P. Smith, Phys. Rev. E **59**, 5655 (1999).
45. J.H. Carpenter, J.-H.J. Cho, B.M. Law, Phys. Rev. E **61**, 532 (2000).
46. H. Zhao, A. Penninckx-Sans, L.-T. Lee, D. Beysens, G. Jannink, Phys. Rev. Lett **75**, 1977 (1995).
47. J.R. Howse, J. Bowers, E. Manzanares-Papayanopoulos, I.A. McLure, R. Steizt, Phys. Rev. E **59**, 5577 (1999).
48. S. Dietrich, R. Schack, Phys. Rev. Lett. **58**, 140 (1987).
49. J.-H.J. Cho, B.M. Law, Phys. Rev. Lett. **68**, 2070 (2001).
50. N.S. Desai, S. Peach, C. Franck, Phys. Rev. E **52**, 4129 (1995).
51. A. Ciach, A. Maciolk, J. Stecki, J. Chem. Phys. **108**, 5913 (1998).
52. A. Ciach, U. Ritschel, Nuc. Phys. B **489**, 653 (1997).
53. P. Czerner, U. Ritschel, Physica A **237**, 240 (1997).
54. C. Houessou, P. Guenoun, R. Gastaud, F. Perrot, D. Beysens, Phys. Rev. A **32**, 1818 (1985).
55. P. Sibille, Ph.D. thesis, University Pierre et Marie Curie, Paris (1998).
56. E.D. Siggia, B.I. Halperin, P.C. Hohenberg, Phys. Rev. B **13**, 2110 (1976).
57. P. Calmettes, Phys. Rev. Lett. **39**, 1151 (1977).
58. See *e.g.* W.H. Press, B.P. Flannery, S.A. Teukolski, W.T. Vetterlink, *Numerical Recipes* (Cambridge University Press, 1986).